Three-dimensional *P* wave tomography of Deception Island Volcano, South Shetland Islands

D. Zandomeneghi,[1] A. H. Barclay,[2] J. Almendros,[1] J. M. Ibáñez,[1] T. Ben-Zvi,[3] W. S. D. Wilcock,[4] and the TOMODEC Working Group

[1]Instituto Andaluz de Geofísica, University of Granada, Campus de Cartuja, s/n, Granada, 18071, Spain (daria@iag.ugr.es; alm@iag.ugr.es; jibanez@ugr.es)
[2]Lamont-Doherty Earth Observatory, 61 Route 9W, Palisades, NY 10964, USA (barclay@ldeo.columbia.edu)
[3]Department of Earth and Space Sciences, University of Washington, Box 351310, Seattle, WA 98195, USA (tbenzvi@u.washington.edu)
[4]School of Oceanography, University of Washington, Box 357940, Seattle, WA 98195, USA (wilcock@u.washington.edu)

Summary Deception Island (62°59' S, 60°41' W) is an active volcano located in the Bransfield Strait between the Antarctic Peninsula and the South Shetland Islands. It is composed of rocks that date from <0.75 Ma to historical eruptions (1842, 1967, 1969 and 1970). In January 2005 an extensive seismic survey took place in and around the island, to collect high quality data for a *P* wave velocity tomography study. A total of 66 land and 14 ocean bottom seismometers were deployed, and more than 5000 airgun shots were fired. A preliminary three-dimensional inversion of the travel times resolves strong velocity contrasts down to 5 km depth. The most striking feature is the low seismic velocity beneath the caldera floor which represents an extensive region of magma beneath a sediment-filled basin. A low velocity zone to the east of Deception Island corresponds to seafloor sedimentary deposits, and high velocities to the northwest are interpreted as the crystalline basement of the South Shetland Islands platform. We observe NE-SW and NW-SE trends in the tomographic image that are compatible with the regional tectonic directions and suggest that the volcanic evolution of Deception Island is conditioned by Bransfield Basin geodynamics.

Citation: Zandomeneghi, D., A. H. Barclay, J. Almendros, J. M. Ibáñez, T. Ben-Zvi, W. S. D. Wilcock, and the TOMODECc Working Group, Three-dimensional *P* wave tomography of Deception Island Volcano, South Shetland Islands – Online Proceedings of the 10th ISAES X, edited by A. K. Cooper and C. R. Raymond et al., USGS Open-File Report 2007-1047, Extended Abstract 025, 4 p.

Introduction

Deception Island is an active volcano located in the Bransfield Strait between the Antarctic Peninsula and the South Shetland Islands. It is a stratovolcano with a basal diameter of ~30 km, and rises ~1500 m from the seafloor to a maximum height of over 500 m above sea level. The 15 km-diameter emerged island is horseshoe-shaped with a flooded inner bay, accessible to the ocean through a 500 m-wide passage. Although heavily studied and frequently visited, the origin of Deception Island volcano is poorly understood: it has a complicated tectonic setting and its geochemistry and seismic activity do not fit any unique interpretation in the framework of the regional geodynamics.

The volcano sits between the central and western sub-basins of the Bransfield Basin, an active marginal rift that separates the South Shetland Islands from the Antarctic Peninsula. The extension, which is propagating along the basin axis from NE to SW, is attributed to rollback of the Phoenix Plate (Barker and Austin, 1998, Jin et al., 2002; Christeson et al., 2003; Vuan et al., 2005 and references therein) and/or transtension due to the left-lateral motion between the Antarctic and Scotia Plates (Klepeis and Lawver, 1992; Rey et al., 1995; Lawver et al., 1996; Gonzalez-Casado et al., 1999; Maestro et al., 2007). The Central Bransfield Basin (CBB) has a broad, axis-parallel neovolcanic zone of seamounts and volcanic ridges but seafloor spreading has not initiated (Christeson et al., 2003). Between the neovolcanic zone and the South Shetland Islands there are large NW-SE trending normal faults that control the extension of several depocenters and have a strike-slip component that offsets the neovolcanic zone toward the South Shetland margin (Gracia et al., 1996; Barker and Austin, 1998; Prieto et al., 1998; Christeson et al., 2003).

Deception Island is composed of volcanic rocks (pyroclastites, agglomerates, tuff and ash) that date from <0.75 Ma to historical eruptions (1842, 1967, 1969 and 1970). Traditionally (Smellie, 2002 and references therein) the volcanic rocks of Deception Island are grouped into pre- and post-caldera formations, assuming that a major caldera-forming event took place. Otherwise, it has been proposed (Rey et al., 1995; Maestro et al., 2007) that the inner bay (Port Foster) formed progressively by passive extension along sets of normal faults that cut the island. In fact, structural mapping and seismic reflection studies within Port Foster show that the local tectonics are controlled primarily by two fault systems (Paredes et al., 2006; Maestro et al., 2007). A NE-SW striking system, consistent with the regional extensional regime of the Bransfield Strait, controls the alignment of the eruptive centers of 1969 and 1970. The second system strikes NNW-SSE, approximately perpendicular to the first one, is observed in fault orientations and may control the shape of Costa Recta, the eastern coast of Deception Island (Fernandez-Ibanez et al., 2005).

The present volcanic activity of Deception Island is high, and includes vigorous hydrothermal circulation (Marti and Baraldo, 1990; Caselli et al., 2004), resurgence of the floor of Port Foster (Cooper et al., 1998) and intense seismicity (Alguacil et al., 1999), that includes volcano-tectonic (Ibañez et al., 2003) and long-period signals (Almendros et al., 1997). These observations, together with gravity and magnetic anomalies (Muñoz-Martin et al., 2005) and high seismic attenuation (Vila et al., 1995), point to the existence of a shallow magma chamber underlying Port Foster, emplaced in a highly fractured medium. The volcano-tectonic activity, which clusters in swarms, is attributed to the action of the major fault systems of the island (Vila et al., 1995; Ibañez et al., 2000). The source mechanism of the long period

activity points to the interaction of thaw water or a shallow aquifer with high-temperature rocks, that is focused along the high-permeability fracture systems (Almendros et al., 1997).

Our understanding of Deception Island is severely limited by the incomplete knowledge of its internal structure. Active-source seismic experiments have been limited to shallow seismic reflection experiments inside Port Foster (Rey et al., 1997) and to larger-scale experiments within the Bransfield Strait (Ashcroft, 1972; GRAPE Team, 1990; Grad et al., 1992; Barker and Austin, 1994; Jin et al., 2002; Christeson et al., 2003). Without information on the distribution of melt, the depth of sediments and the location of intrusive bodies and fault zones beneath and around the island, models for the structure and evolution of Deception Island are poorly constrained. To address this problem, a three-dimensional seismic *P* wave tomography survey of Deception Island volcano was conducted as part of the TOMODEC project in January, 2005.

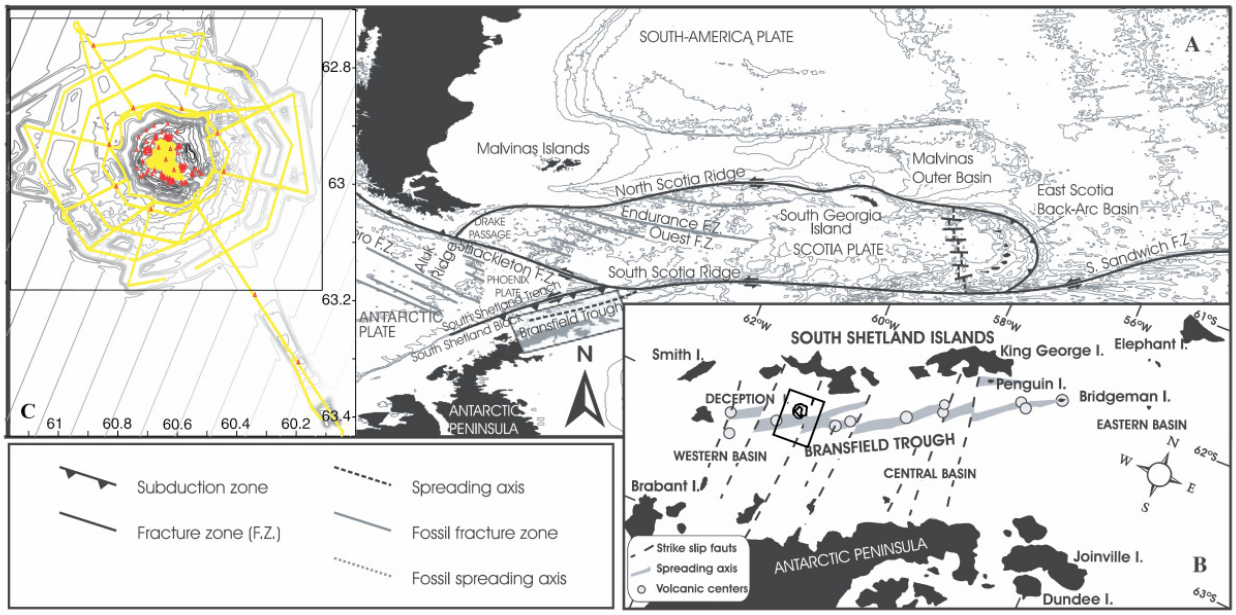

Figure 1. (A) Regional tectonic map of Southwest Atlantic Region. (B) Location of Deception Island within the Bransfield Strait. (C) Experiment area with shot positions in yellow and receivers in red. Area of map is given by box in (B). Modified from Maestro et al., 2007.

Seismic experiment, data and method

Sixty-six land and 14 ocean-bottom seismometers (OBSs) were used to record >5000 airgun shots from the *R/V Hespérides*. The land stations (autonomous seismometers and arrays) were distributed over the accessible areas of Deception Island, and the OBSs were deployed within the inner bay and in a circular configuration around the island. Airgun shots were fired every minute in a grid pattern inside Port Foster and approximately every two minutes along five concentric rings and two long lines outside the island (Figure 1). The shooting patterns were repeated and some stations were relocated between the first and second rounds. Most of the seismometers were vertical component only, but the OBSs and 20 stations were equipped with 3-component sensors; the OBSs also included a hydrophone.

More than 70,000 *P* wave travel times were picked and then inverted using the method of Toomey et al. (1994). This approach is particularly well suited for the Deception Island experiment because it includes topography, bathymetry, and the water-path in the calculation. We inverted the data using two grid configurations in order to understand the tradeoff between raytracing accuracy and computational time. The first configuration was a large grid that was centered on Deception Island and extended 53 km and 52 km in the E-W and N-S directions, respectively. The ray-tracing grid had a spacing of 250 m and the perturbational grid 500 m; both grids extended to 12 km depth. For the second configuration, we reduced the grid dimensions to 12 x14 x 7 km (to the region around Port Foster) and the raytracing and perturbational grid spacings to 100 m and 200 m, respectively. Although the raytracing accuracy was poorer for the sparser raytracing grid, we concluded after comparison of the inversion results within Port Foster for the two grid configurations that the sparse grid was sufficiently accurate. The depth-dependent starting velocity model was obtained from the horizontal average of the two-dimensional tomographic result (Ben-Zvi et al., this volume) in the region away from the island. The inversions were regularized using the best combination of damping and smoothing that simultaneously minimized the data misfit, model roughness, and model variance. We used checkerboard, spread-function and other hypothesis tests to understand the spatial and amplitude resolution of the tomographic image.

Results and discussion

Convergence of the tomographic inversion to a stable solution was obtained after 6 iterations, when the root-mean-squared (RMS) data misfit was reduced by 80% from 247 ms for the starting model to 52 ms. For the denser grid, the inversion result was also stable after 6 iterations, with a RMS reduction from 260 ms to 34 ms. Results from both grid configurations were used to interpret the velocity structure of Deception Island and surrounding region.

Figure 2 shows the distribution of Vp in the Deception Island region The tomographic image is highly heterogeneous with a lateral variation of > 2 km/s at 1 km depth (Figure 2), and similar contrasts are present between the surface and 5 km depth, for both grid configurations. Although *P* wave velocities cannot generally be interpreted uniquely, our interpretation of the image is aided by the spatial association of many of the anomalies with known structures. In addition, our resolution testing demonstrates that the major anomalies in Figure 2 are not artifacts.

A high-velocity region (A1) dominates to the NW of Deception Island at all depths and is separated from the low velocities of the island by a sharp lateral velocity gradient (>0.8 km/s over ~2 km) that is linear with its trend parallel to the Bransfield Strait. This boundary is a continuation of the faulted northern margin of the CBB (Lawver et al., 1996; Barker and Austin, 1994) and likely separates Deception Island and the extended basin from the crystalline basement of the pre-Bransfield continental crust (Christeson et al., 2003). This anomaly reaches its maximum strength between 1 and 3.5 km depth, and it is not horizontally homogeneous. Two of the three maxima that are superimposed on this high-velocity region appear to disrupt the linearity of the boundary; both the southwestern and northeastern anomalies extend across the boundary and may indicate offset along NW-SE-trending faults. Transfer zones with similar strike have been identified elsewhere in the CBB (Barker and Austin, 1994; Christeson et al., 2003) and the presence of similar faults near Deception Island has been proposed (Rey et al., 1995; Munoz-Martin et al., 2005).

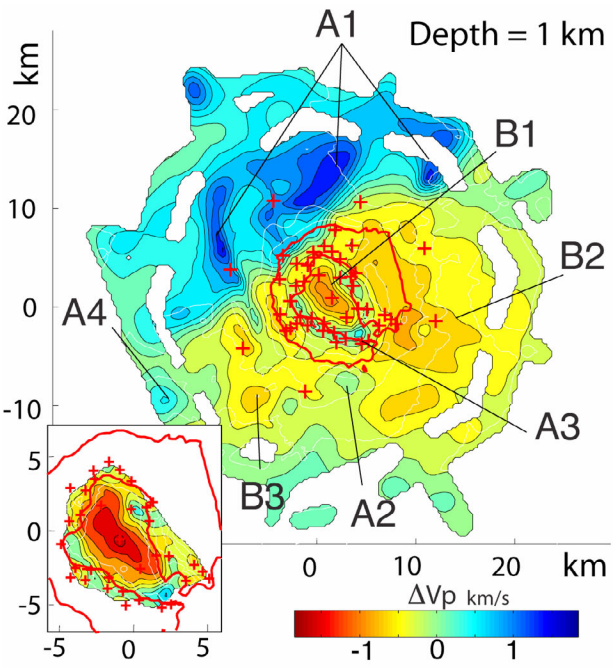

Figure 2. *P* wave velocity perturbations at 1 km depth**.** Coastline of Deception Island is outlined in red. Crosses are position of receivers. Contour interval is 0.2 km/s. Main figure and inset show results for sparse and dense grids, respectively.

The most pronounced low velocity anomaly (B1) lies beneath Port Foster, across the whole resolved depth range. At 1 km, the anomaly is aligned NW-SE and its maximum perturbation exceeds 1 km/s with respect to the starting structure (Figure 2). The Port Foster basin is filled with at least 1.2 km of sediments (Grad et al., 1992; Ben-Zvi et al., this volume) and hosts a vigorous geothermal system as inferred from geochemical and geophysical observations (Marti and Baraldo, 1990; Caselli et al., 2004; Almendros et al., 1997). At 0-0.5 km depth the anomaly is composed of several maxima and some coincide with the location of the 1967 and 1970 eruption centers. The amplitude and depth of the anomaly cannot be explained by thicker sediments alone (Ben-Zvi et al., this volume) and also requires high temperatures and partial melt located beneath Port Foster at depths greater than 2 km. The presence of a magma reservoir beneath Port Foster has been suggested by a number of previous studies (Ibañez et al., 2003; Vila et al., 1995).

The low velocity anomaly within Port Foster is partially surrounded by a horseshoe-shaped pattern of high velocities (A3) that approximately follows the coast and persists in our image from the surface to ~3 km depth. These high velocities, which are in a particularly well-resolved region, may either correspond to a pre-caldera shield phase of ancient Deception Island, to a previous caldera rim or to frozen, shallow-level intrusions that may have fed earlier eruptions.

Many of the other low- and high-velocity anomalies in the tomographic image can be explained by thicker sedimentary deposits and volcanic features, respectively. The large low-velocity region to the east of Deception Island (B2) corresponds to seafloor that is characterized by sediment transport (gullies, ridges and debris flows) from Deception Island into the CBB. Its overall shape is strongly irregular although the position of the maximum perturbation at 0.5 km depth corresponds to the location of Costa Recta The size and position of high-velocity anomaly A2, which is directly to the south of Deception Island, are similar to that of an isolated Bouguer gravity and magnetization high (Munoz-Martin et al., 2005) and may represent a buried intrusion. We apply a similar interpretation to anomaly A4, which is centered on Sail Rock, an eroded andesitic sea stack located to the SW of Deception Island. By contrast, a low-velocity anomaly that is located to the W of Deception Island (B3) may be related to a nearby region of extensive seafloor volcanism, and may be the expression of thicker volcanoclastic sediments or an active magmatic system.

Summary

A three-dimensional seismic P wave tomographic image of Deception Island volcano shows strong lateral velocity variations that are attributed to a shallow crustal magmatic system beneath Port Foster, as well as frozen intrusive bodies, crystalline basement and sediment thickness variations. A number of these structures have a NW-SE trend and can be interpreted in the context of a regional tectonic framework for the Bransfield Basin, that includes extension in the NE-SW direction in addition to the NW-SE extension of the Bransfield Strait, and suggests an influence of NW-SE-oriented transfer zones in the evolution of Deception Island.

Acknowledgements. We are grateful for the assistance of the officers and crew of the *R/V Hespérides* and *R/V Las Palmas*, and the personnel of the Gabriel de Castilla base. This work was supported by the TOMODECc Project (REN 200-3833) and NSF Award ANT-0230094.

References

Alguacil, G., J. Almendros, E. Del Pezzo, A. Garcia, J. M. Ibañez, M. La Rocca, J. Morales, and R. Ortiz (1999), Observations of volcanic earthquakes and tremor at Deception Island, Antarctica, Annali di Geofisica, 42, 417-436.

Almendros, J., J. Ibañez, G. Alguacil, E. Del Pezzo, and R. Ortiz (1997), Array tracking of the volcanic tremor source at Deception Island, Antarctica, Geophys. Res. Lett., 24, 3069-3072.

Ashcroft, W. A. (1972), Crustal structure of the South Shetland Islands and Bransfield Strait. British Antarctic Survey Scientific Reports, 66.

Barker, D. H., and J. A. Austin (1994), Crustal diapirism in Bransfield Strait, West Antarctica: evidence for distributed extension in marginal-basin formation, Geology, 22, 657-660.

Barker, D. H. N., and J. A. Austin (1998), Rift propagation, detachment faulting, and associated magmatism in Bransfield Strait, Antarctic, J. Geophys. Res., 103, 24,017-24,043.

Ben-Zvi, T., W. S. D. Wilcock, A. H. Barclay, D. Zandomeneghi, J. M. Ibáñez, J. Almendros, and the TOMODEC Working Group (this volume), The P-wave velocity structure of Deception Island, Antarctica, from two-dimensional seismic tomography.

Caselli, A. T., M. Santos-Afonso, and M. R. Agusto (2004), Gases fumarolicos de la isla Decepcion (Shetland del Sur, Antartida): variaciones quimicas y depositos vinculados a la crisis sismica de 1999, Rev. As. Geol. Arg., 59, 291-302.

Christeson, G. L., H. N. Barker, J. A., Austin, and W. D. Dalziel (2003), Deep crustal structure of Bransfield Strait; initiation of a back arc basin by rift reactivation and propagation, J. Geophys. Res, 108, 2492, doi:10.1029/2003JB002468.

Cooper, A. P. R., J. L. Smellie, and J. Maylin (1998), Evidence for shallowing and uplift from bathymetric records of Deception Island, Antarctica, Antarctic Science, 10, 455-461.

Fernandez-Ibanez, F., R. Perez-Lopez, J. J. Martinez-Diaz, C. Paredes, J. L. Giner-Robles, A. T. Caselli, and J. M. Ibañez (2005), Costa Recta Beach, Deception Island, West Antarctica; a retreated scarp of a submarine fault? Antarctic Science, 17, 418-426.

Gonzalez-Casado, J. M., J. Lopez-Martinez, J. Giner, J. J. Duran, and P. Gumiel (1999), Analisis de la microfracturacion en la Isla Decepcion, Antartida Occidental, Geogaceta, 26, 27-30.

Gracia, E., M. Canals, M. L. Farran, M. J. Prieto, and J. Sorribas (1996), Morphostructure and Evolution of the Central and Eastern Bransfield Basins (NW Antarctic Peninsula), Mar. Geophys. Res., 18, 429-448.

Grad, M., A. Guterch, and P. Sroda (1992), Upper crustal structure of Deception Island area, Bransfield Strait, West Antarctica, Antarctic Science, 4, 469-476.

GRAPE Team (1990), Preliminary results of seismic reflection investigations and associated geophysical studies in the area of the Antarctic Peninsula, Antarctic Science, 2, 223-234.

Ibañez, J., P. Morales, G. Alguacil, J. Almendros, R. Ortiz, E. Del Pezzo, M. La Rocca, and A. Garcia (2000), Seismovolcanic signals at Deception Island volcano, Antarctica: wave field analysis and source modeling, J. Geophys. Res., 135, 13,905-13,931.

Ibañez, J. M., J. Almendros, E. Carmona, C. Martinez-Arevalo, and M. Abril (2003), The recent seismo-volcanic activity at Deception Island volcano, Deep-Sea Research, 50, 1611-1629.

Jin, Y. K., R. D. Larter, Y. Kim, S. H. Nam, and K. J. Kim (2002), Seismic structure of the western Bransfield Strait, Antarctic Peninsula: rift propagation from northeast to southwest, in, Antarctica at the close of the millennium, Royal Society of the New Zealand Bulletin, 35, 499-506.

Klepeis, K. A., and L. A. Lawver (1992), Tectonics of the Antarctic -Scotia plate boundary near Elephant and Clarence Islands, West Antarctica, J. Geophys. Res., 101, B9, 20,211-20,231.

Lawver, L. A., M. Ghidella, R. P. Von Herzen, R. A. Keller, G. P. Klinkhammer, and C. S. Chin (1996), Distributed, active extension in Bransfield Basin, Antarctic Peninsula; evidence from multibeam bathymetry, GSA Today, 6, 1-6.

Maestro, A., L. Somoza, J. Rey, J. Martinez-Frias, and J. Lopez-Martinez (2007), Active tectonics, fault patterns and stress field of Deception Island: a response to oblique convergence between the Pacific and Antarctic Plates, *submitted,* J. South Am. Earth Sci..

Marti, J., and A. Baraldo (1990), Pre-caldera pyroclastic deposits of Deception Island (South Shetland Islands), Antarctic Science, 2, 4, 345-352.

Munoz-Martin, A., M. Catalan, J. Martin-Davila, and A. Carbo (2005), Upper crustal structure of Deception Island area (Bransfield Strait, Antarctica) from gravity and magnetic modeling, Antarctic Science, 17, 213-224.

Paredes, C., R. Perez-Lopez, J. L Giner-Robles, R. de la Vega, A. Garcia-Garcia, and P. Gumiel (2006), Distribucion espacial y zonificacion tectonica de los morfolineamentos en la Isla Decepcion (Shetland del Sur, Antartida), Geogaceta, 39, 75-78.

Prieto, M. J., M. Canals, G. Ercilla, and M. de Batist (1998), Structure and geodynamic evolution of the Central Bransfield Basin (NW Antarctica) from seismic reflection data, Marine Geol., 149, 17-38.

Rey, J., L. Somoza, and J. Martinez-Frias (1995), Tectonic, volcanic and hydrothermal event sequence on Deception Island (Antarctica). Geo-Marine Lett., 15, 1-8.

Rey, J., L. Somoza, J. Martinez-Frías, R. Benito, and S. Martín-Alfageme (1997), Deception Island (Antarctica): a new target for exploration of Fe-Mn mineralization? in, Manganese Mineralization: geochemistry and mineralogy of terrestrial and marine deposits, edited by K. Nicholson et al., Geological Society Special Publication No. 119, 239-251.

Smellie, J. L. (2002), Geology, in, Geology and geomorphology of Deception Island., edited by J. L. Smellie et al., British Antarctic Survey Geomap Series, Cambridge, United Kingdom.

Toomey, D. R., S. C. Solomon, and G. M. Purdy (1994), Tomographic imaging of the shallow crustal structure of the East Pacific Rise at 9˚30' N, J. Geophys. Res., 99, B12, 24,135-24,157.

Vila, J., A. M. Correig, and J. Marti (1995), Attenuation and source parameters at Deception Island (South Shetland Islands, Antarctica), PAGEOPH, 144, 2, 229-250.

Vuan, A., S. D. Robertson, D. A. Wiens, and G. F. Panza (2005), Crustal and upper mantle S-wave velocity structure beneath the Bransfield Strait (West Antarctica) from regional surface wave tomography, Tectonophysics, 397, 241-259.